

# Measurement of the Bistatic Scattering Coefficient over Wide Angular Ranges Using SAR on Unmanned Aerial Vehicles

Thomas Börner and Michelangelo Villano

German Aerospace Center (DLR), Microwaves and Radar Institute, Germany

## Abstract

Bistatic radar imaging has been an important topic ever since radar scattering and imaging has been made possible. Nowadays, Unmanned Aerial Vehicle (UAV)-based synthetic aperture radar (SAR) systems open up a completely new space for measurements that have not been carried out before. UAVs not only enable very accurate and cost-effective monitoring of local areas with unprecedentedly short revisit intervals, but also the use of configurations with large bistatic angles, which are of difficult implementation for spaceborne and airborne systems and have been so far used only in the context of ground-based (surveillance) radars. This paper shows how to measure the bistatic scattering coefficient of a surface over wide ranges of bistatic angles using a SAR mounted on UAVs. Starting from the necessary, basic geometrical definitions, it is shown how to choose geometrical configurations to achieve specific bistatic angles under the constraints of desired ground resolution and ground area coverage, while at the same time avoiding ambiguities. Moreover, the feasible bistatic angular coverage for a ground target is analysed such that conclusions can be drawn about how to maximise this coverage for given measurement scenarios. This analysis prepares for the execution of field demonstration and measurements with UAVs aiming at fully characterizing the bistatic scattering of surfaces of interest.

## 1 Introduction

Space- and airborne synthetic aperture radar (SAR) systems are used for many different applications in the field of Earth observation [1]. However, when it comes to exploiting bistatic scattering, these systems have been so far mostly limited to very small bistatic angles [2]. Even the few airborne demonstrations only covered small baselines in the backscattering regime (e.g., [3]). By using unmanned aerial vehicles (UAVs), such as drones or multicopters [4]-[6], it is much easier to enable not only bistatic backscatter, but also forward scatter measurements with arbitrary bistatic angles that have not yet been demonstrated, at least not in agile airborne configurations. Ground-based (surveillance) radars [7] do make use of such bistatic angles, but the sensor positions are fixed, and the targets are moving. UAV-based SAR systems are very flexible, cost-effective, easy to deploy, and enable frequent monitoring of local areas. Hence, they are very attractive for rather easily demonstrating new techniques and concepts. Classical techniques like high-resolution SAR imaging, SAR interferometry and the generation of digital elevation models (DEMs) have already been demonstrated on UAV-based systems, but not bistatic measurements. This paper therefore aims at theoretically exploring capabilities and restrictions of bistatic configurations in preparation for future demonstrations and measurements.

At first some basic geometrical considerations will be made to establish a clear mathematical definition and understanding of the bistatic configuration (see section 2). In particular constraints due to ground resolution, swath position and the avoidance of range ambiguities will be taken into account. This will lead to establishing a geometrical space of possible practical solutions, i.e., possible flight and sensor configurations (see section 3). In a last step the bistatic angular coverage will be examined (see section 4), since this is of particular importance for measurements of objects on the ground. The goal should be to see a ground target under many different bistatic angles with relatively few observations.

## 2 Basic geometrical considerations

For a start let us consider two radar sensor platforms (e.g., drones) flying in a geometric configuration that enables bistatic imaging. To make things easier we restrict the geometry to a plane, setting the bistatic scattering angle  $\phi$  to zero degrees, as shown in **Figure 1**. The variation of the azimuthal bistatic angle (not represented in Figure 1) will be obtained by exploiting the synthetic aperture principle, if one of the platforms is fixed and the other is flying in a direction perpendicular to the plane represented in Figure 1. The setup shall currently also be limited to forward scattering. Bistatic backscattering will be investigated at a later stage.

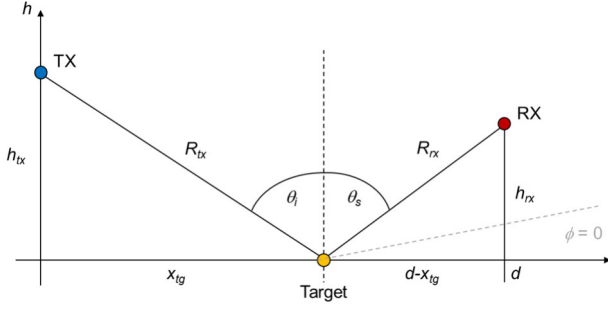


**Figure 1** Basic geometrical setup with two radar sensors (TX: transmitter, RX: receiver) and an arbitrary target point on the ground.

The transmitter (TX) height over ground is  $h_{tx}$ , the receiver (RX) height is  $h_{rx}$ , the range distances from TX and RX to the target are  $R_{tx}$  and  $R_{rx}$ , respectively, and the incidence and scattering angles are  $\theta_i$  and  $\theta_s$ . If the horizontal distance from the transmitter to the target is  $x_{tg}$ , the horizontal distance from the receiver to the target is given by  $d - x_{tg}$ , where  $d$  is the horizontal distance from the transmitter to the receiver, and  $x_{tg} \in [0; d]$ .

Knowing the position of the sensors and the target, the remaining variables can be calculated as follows:

$$R_{tx} = \sqrt{h_{tx}^2 + x_{tg}^2} \quad (1)$$

$$R_{rx} = \sqrt{h_{rx}^2 + (d - x_{tg})^2} \quad (2)$$

$$\theta_i = \tan^{-1}\left(\frac{x_{tg}}{h_{tx}}\right) \quad (3)$$

$$\theta_s = \tan^{-1}\left(\frac{d - x_{tg}}{h_{rx}}\right) \quad (4)$$

The bistatic range distance from transmitter to receiver is  $R = R_{tx} + R_{rx}$ . In order to find the minimum bistatic range distance the derivative of  $R$  with respect to  $x$  can be evaluated and set to zero:

$$\frac{dR}{dx} = \frac{x}{R_{tx}} - \frac{d - x}{R_{rx}} \quad (5)$$

Another important variable to take into account is the range resolution that depends on the geometry and the radar signal bandwidth  $B_{rg}$ . In a classical monostatic radar the slant range resolution  $\delta_{rg}$  is given as

$$\delta_{rg} = \frac{c}{2B_{rg}}, \quad (6)$$

whereas in a bistatic configuration the slant range resolution  $\delta_{rg,bist}$  is “doubled”:

$$\delta_{rg,bist} = \frac{c}{B_{rg}} \quad (7)$$

However, in most cases we are interested in the bistatic ground range resolution  $\delta_{rg,G,bist}$ , i.e., we need to project the bistatic slant range resolution of (7) to the ground by dividing it by the derivative in eq. 5:

$$\delta_{rg,G,bist} = \frac{c}{B_{rg} \cdot \left(\frac{x}{R_{tx}} - \frac{d - x}{R_{rx}}\right)} \quad (8)$$

Now let us also introduce additional geometrical parameters defining the radar, namely the elevation beam width of the transmitting and receiving antennas,  $\psi_i$  and  $\psi_s$ , as shown in **Figure 2**. These parameters define the illuminated ground swathes. Only the overlapping area (let us call it the “bistatic swath”) can be seen by both, transmitter and receiver and is therefore of interest for bistatic measurements.

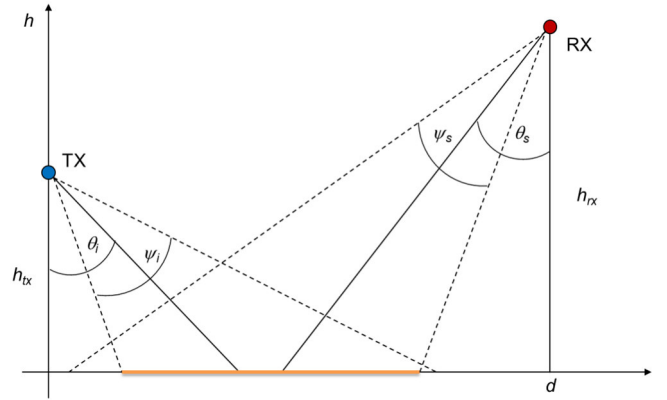


**Figure 2** TX and RX beam width and the according ground swathes. The orange line depicts the overlapping area.

The formulae derived above and an arbitrary set of geometrical parameters can be used to compute an exemplary behavior of bistatic range, resolution, and the according position of the bistatic swath, which is shown in **Figure 3**. In agreement with the theory, the resolution is worst at the position corresponding to the minimal bistatic range.

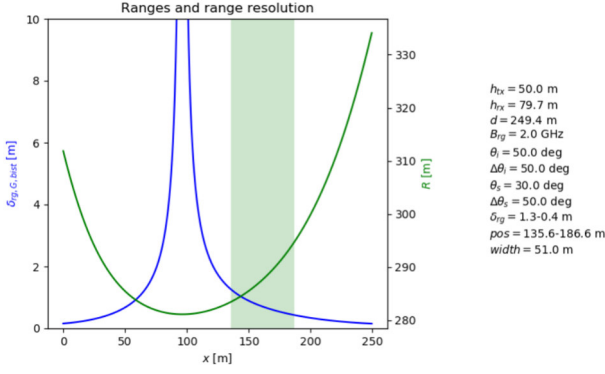


**Figure 3** Bistatic range (green line), bistatic ground range resolution (blue line) and the position of the bistatic swath (light green area) for a given set of input parameters.

In this particular example it can be seen that the bistatic swath is at a position, where every point on the ground has a different bistatic range, i.e., the points can be distinguished from each other when processing the acquired radar data. Problems will occur when the bistatic swath extends to both sides of the minimal bistatic range, because the points on either side will have the same ranges and therefore cannot be resolved from each other, generating an ambiguity. In this context, it is important to point out that typical radar systems mounted on drones are characterized by wide elevation beams in the order of  $60^\circ$ . This means that in order to properly prepare a measurement scenario, geometries should be chosen such that the aforementioned ambiguities are avoided. Of course, this could be done via trial and error until a good solution is found. However, certainly there is a better way, namely to find mathematical (geometrical) conditions that define the boundaries of the space of solutions, which is going to be discussed in the following.

### 3 Geometrical solution space

As a first condition, the TX and RX swathes have to overlap. The TX ground swath beginning and end points shall be defined as  $x_{i1}$  and  $x_{i2}$ , whereas for the RX swath they are denoted  $x_{s1}$  and  $x_{s2}$ , respectively. There is an overlap if either

$$x_{s2} > x_{i1} \quad (9)$$

or

$$x_{i2} > x_{s1}. \quad (10)$$

The first condition given in (9) leads to

$$d - h_{rx} \tan\left(\theta_s - \frac{\psi_s}{2}\right) > h_{tx} \tan\left(\theta_i - \frac{\psi_i}{2}\right) \quad (11)$$

and thus

$$h_{rx} < \frac{d - h_{tx} \tan\left(\theta_i - \frac{\psi_i}{2}\right)}{\tan\left(\theta_s - \frac{\psi_s}{2}\right)}. \quad (12)$$

The second condition given in (10) provides us with

$$d - h_{rx} \tan\left(\theta_s + \frac{\psi_s}{2}\right) < h_{tx} \tan\left(\theta_i + \frac{\psi_i}{2}\right) \quad (13)$$

and thus

$$h_{rx} > \frac{d - h_{tx} \tan\left(\theta_i + \frac{\psi_i}{2}\right)}{\tan\left(\theta_s + \frac{\psi_s}{2}\right)}. \quad (14)$$

In order to avoid ambiguities, the bistatic swath has to be entirely on either one or the other side of the bistatic range minimum. Setting eq. (5) to zero gives us the position of the minimum at

$$x_{Rmin} = \frac{h_{tx} \cdot d}{h_{tx} + h_{rx}}. \quad (15)$$

In case the bistatic swath is on the right side of the minimum (let us call this “right branch”), the lower  $x$ -coordinate of the swath  $x_l$  has to be greater than  $x_{Rmin}$ , and if it is on the left side (“left branch”), the upper  $x$ -coordinate  $x_u$  has to be smaller than  $x_{Rmin}$ , i.e.:

$$x_l > x_{Rmin} \quad \text{or} \quad x_u < x_{Rmin} \quad (16)$$

where

$$x_l = \begin{cases} x_{s1} & \text{for } x_{i1} < x_{s1} \\ x_{i1} & \text{for } x_{i1} > x_{s1} \end{cases} \quad (17)$$

and

$$x_u = \begin{cases} x_{i2} & \text{for } x_{i2} < x_{s2} \\ x_{s2} & \text{for } x_{i2} > x_{s2} \end{cases} \quad (18)$$

This leads us to the following conditions, if the swath lies on the right side of the minimum (“right branch”):

$$h_{rx} > \frac{d}{\tan\left(\theta_i - \frac{\psi_i}{2}\right)} - h_{tx} \quad (19)$$

$$h_{rx} > \frac{d}{\tan\left(\theta_s + \frac{\psi_s}{2}\right)} - h_{tx} \quad (20)$$

In case the swath lies on the left side of the minimum (“left branch”), the following alternative conditions hold:

$$h_{rx} < \frac{d}{\tan\left(\theta_i + \frac{\psi_i}{2}\right)} - h_{tx} \quad (21)$$

$$h_{rx} < \frac{d}{\tan\left(\theta_s - \frac{\psi_s}{2}\right)} - h_{tx} \quad (22)$$

In **Figure 4** the transmitter height is fixed to 50 m while the receiver height and the distance of transmitter and receiver are varying. Here we are looking for right branch solutions, i.e., conditions provided in eqs. (12), (14), (19), and (20) must hold. If we choose a TX-RX distance and an RX height in the green area, we can be sure to have overlapping swathes and no ambiguities.

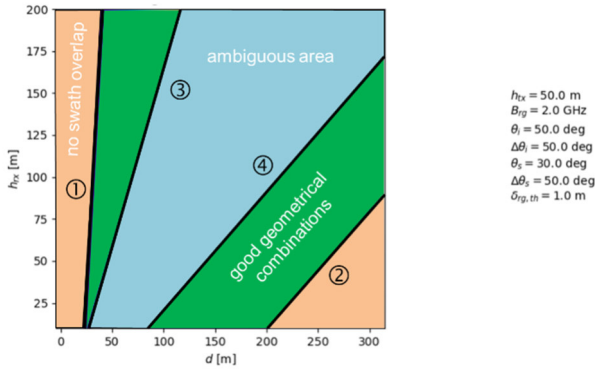


**Figure 4** Exemplary solution space for a given set of input parameters. Orange denotes areas where there is no swath overlap between TX and RX, light blue denotes the area where we have ambiguities, and green denotes areas with good geometrical combinations of measurement/flight parameters.

## 4 Bistatic angular coverage

Now that we have the ability to find proper bistatic imaging configurations, we want to find those that are suited for measuring target properties, i.e., to characterize the bistatic scattering over wide angular ranges. The bistatic angle plays an important role, i.e., the scattering of a target strongly depends on the incident and scattered angles. In general, a physical description of the target gets better the more different bistatic angles you are using throughout the measurement. In **Figure 5** an example is shown of how the incident and scattered angles are correlated to the chosen imaging geometry. In the left plot the distance is varied while keeping the RX and TX height constant, whereas the right plot keeps a constant distance and varies the RX height. However, this case does not take into account the conditions for avoiding ambiguities. It shall only show the general relations.

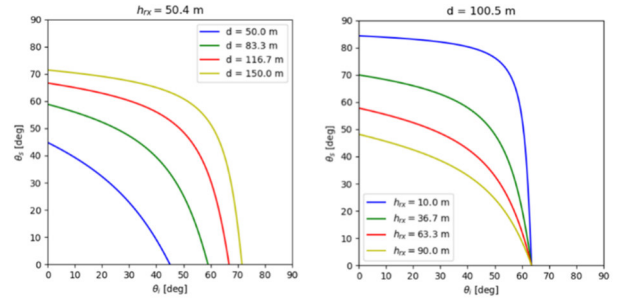


**Figure 5** Left: Incident vs. scattered angles with a fixed RX height of 50.4 m and varying RX to TX distances. Right: Incident vs. scattered angles with a fixed RX to TX distance while varying the RX height. The TX height is fixed at 50 m in both cases.

Let us now make an example taking into account valid bistatic imaging conditions (common swath and no ambiguities). Within the solution space we pick solutions in a regularly spaced grid, and for those, incident vs. scattered angles are plotted. In addition, also the bistatic angle  $\theta_i + \theta_s$  is plotted vs. the position within the swath. As can be seen in **Figure 6** the possible angular range is quite limited for this particular configuration. Incidence angles between  $0^\circ$  and  $30^\circ$  as well as  $50^\circ$  and  $60^\circ$  are not possible at all, neither are scattered angles between  $0^\circ$  and  $10^\circ$  and above  $60^\circ$ . By changing the TX height and RX and TX look angles, the gaps can be partly filled (see **Figure 7**). However, there will not be a single optimal configuration for covering a mostly complete set of bistatic angles. It will be a combination of a few to several configurations, also strongly depending on the type of target (e.g., distributed target, point like scatterer, geometrically complex targets, etc.) and other constraints (e.g. weather conditions, restricted flight heights, etc.). Caveat: there are also technical and radar specific constraints like radiometric resolution, signal power, noise, side lobes, etc. that have to be taken care of. Not every geometrically valid configuration will provide radar data with sufficient quality. Hence there will be quite a number of trade-offs to be made for every individual measurement.

The examples in **Figure 6** and **Figure 7** do only consider solutions for the right branch. Including left branch solutions opens up an even broader range of possible bistatic angles.

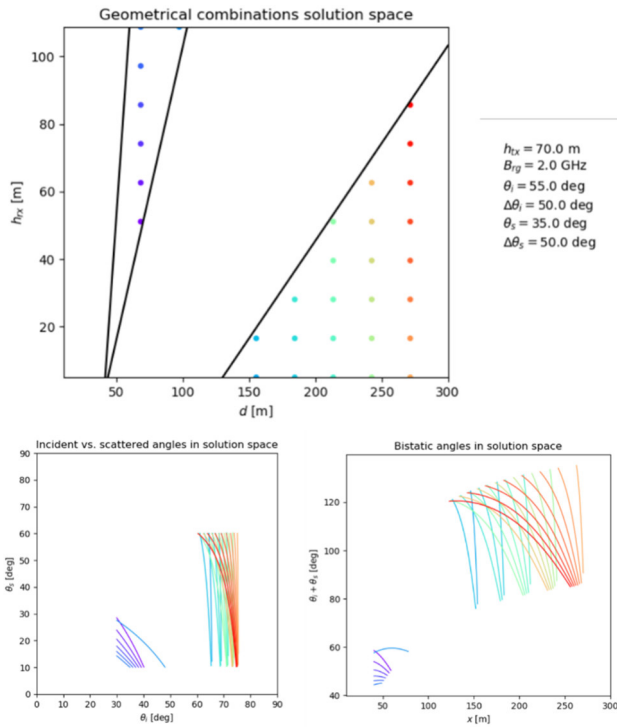


**Figure 6** Top: Solution space for a given set of parameters. The grid point colors are reflected as lines in the following plots. Lower left: Incident vs. scattered angles, and lower right: bistatic angle over ground range.

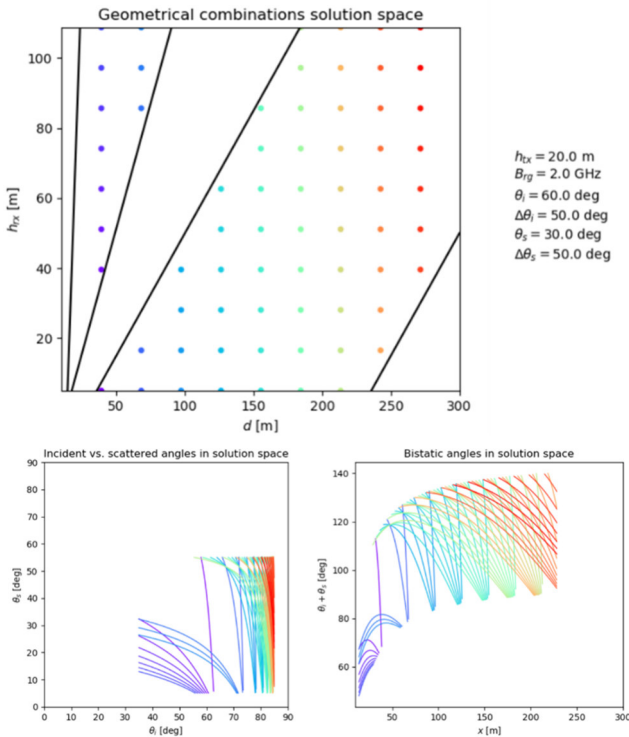


**Figure 7** Top: Solution space for a given set of parameters. The grid point colors are reflected as lines in the following plots. Lower left: Incident vs. scattered angles, and lower right: bistatic angle over ground range.

## 5 Conclusions and Outlook

This work provides a first insight into the measurement of the bistatic backscatter coefficient over wide ranges of bistatic angles using UAVs. Starting from the description of the geometry, it establishes the main relationships between the bistatic angles and the geometric parameters. It also discusses the constraints imposed by ambiguities and the need of an overlapping swath, which are critical for systems with wide beam width, as it is the case of radar mounted on UAVs. The outcome of the analysis is a plot with the allowed regions for all possible combinations of the (fixed) transmitter height and the horizontal distance between transmitter and receiver. For some exemplary configurations the bistatic angles that can be measured are shown. The work can be easily extended to the case of bistatic backscatter as well as to systems flying at larger heights. Further analyses will build up on this work and determine how to measure a wide range of bistatic angles under the constraint of a reduced number of flights.

## 6 Acknowledgements

This work was partially funded by the European Union (ERC, DRITUCS, 101076275). Views and opinions expressed are however those of the authors only and do not necessarily reflect those of the European Union or the European Research Council Executive Agency. Neither the European Union nor the granting authority can be held responsible for them.

## 7 Literature

- [1] Moreira, A., Prats-Iraola, P., Younis, M., Krieger, G., Hajnsek, I., Papathanassiou, K.P.: A tutorial on synthetic aperture radar. *IEEE Geosci. Remote Sens. Mag.*, vol. 1, no. 1, pp. 6-43, Mar. 2013.
- [2] Baumgartner, S.V., et al.: Bistatic Experiment Using TerraSAR-X and DLR's new F-SAR System. 7th European Conference on Synthetic Aperture Radar, Friedrichshafen, Germany, 2008.
- [3] Meta, A., et al.: Bistatic Airborne SAR Acquisitions at L-Band by MetaSensing: First Results. EUSAR 2018; 12th European Conference on Synthetic Aperture Radar, Aachen, Germany, 2018.
- [4] Hügler, P., Roos, F., Schartel, M., Geiger, M., Waldschmidt, C.: Radar Taking Off: New Capabilities for UAVs. *IEEE Microwave Magazine*, vol. 19, no. 7, pp. 43-53, Nov.-Dec. 2018.
- [5] Grathwohl, A., et al.: Taking a Look Beneath the Surface: Multicopter UAV-Based Ground-Penetrating Imaging Radars. *IEEE Microwave Magazine*, vol. 23, no. 10, pp. 32-46, Oct. 2022.
- [6] Villano, M., et al.: Potential of Multi-Static SAR Systems for Earth Monitoring and Their Demonstration

Using Swarms of Drones. IGARSS 2023, Pasadena, CA, USA, 16-21 July 2023.

- [7] Ritchie, M., Fioranelli, F., Griffiths, H., Torvik, B.: Monostatic and Bistatic Radar Measurements of Birds and Micro-Drone. IEEE Radar Conference (Radar-Conf), 2016.